Optic Nerve Head Astrocytes Display Axon-Dependent and -Independent Reactivity in Response to Acutely Elevated Intraocular Pressure

Shandiz Tehrani, Lauren Davis, William O. Cepurna, R. Katherine Delf, Diana C. Lozano, Tiffany E. Choe, Elaine C. Johnson, and John C. Morrison

Casey Eye Institute, Department of Ophthalmology, Oregon Health & Science University, Portland, Oregon, United States

Correspondence: Shandiz Tehrani, Department of Ophthalmology, Casey Eye Institute, Oregon Health & Science University, 3375 SW Terwilliger Boulevard, Portland, OR 97239-4197, USA; tehrani@ohsu.edu.

Submitted: August 3, 2018
Accepted: December 21, 2018

Citation: Tehrani S, Davis L, Cepurna WO, et al. Optic nerve head astrocytes display axon-dependent and -independent reactivity in response to acutely elevated intraocular pressure. *Invest Ophthalmol Vis Sci*. 2019;60:312–321. https://doi.org/10.1167/iovs.18-25447

Purpose. Optic nerve head (ONH) astrocytes provide support for axons, but exhibit structural and functional changes (termed reactivity) in a number of glaucoma models. The purpose of this study was to determine if ONH astrocyte structural reactivity is axon-dependent.

Methods. Using rats, we combine retrobulbar optic nerve transection (ONT) with acute controlled elevation of intraocular pressure (CEI), to induce total optic nerve axon loss and ONH astrocyte reactivity, respectively. Animals were euthanized immediately or 1 day post CEI, in the presence or absence of ONT. ONH sections were labeled with fluorescent-tagged phalloidin and antibodies against β3 tubulin, phosphorylated cortactin, phosphorylated paxillin, or complement C3. ONH label intensities were quantified after confocal microscopy. Retrobulbar nerves were assessed for axon injury by light microscopy.

Results. While ONT alone had no effect on ONH astrocyte structural orientation, astrocytes demonstrated significant reorganization of cellular extensions within hours after CEI, even when combined with ONT. However, ONH astrocytes displayed differential intensities of actin (phosphorylated cortactin) and focal adhesion (phosphorylated paxillin) mediators in response to CEI alone, ONT alone, or the combination of CEI and ONT. Lastly, label intensities of complement C3 within the ONH were unchanged in eyes subjected to CEI alone, ONT alone, or the combination of CEI and ONT, relative to controls.

Conclusions. Early ONH astrocyte structural reactivity to elevated IOP is multifaceted, displaying both axon dependent and independent responses. These findings have important implications for pursuing astrocytes as diagnostic and therapeutic targets in neurodegenerative disorders with fluctuating levels of axon injury.

Keywords: optic nerve head, astrocyte reactivity, axon, elevated intraocular pressure, glaucoma

Astrocytes are local glial cells that provide structural, functional, and developmental support for central nervous system axons.[1–8] Under physiologic conditions, astrocytes display a stellate morphology in vivo, with numerous actin-rich extensions that envelop and surround axons.[9–11] However, astrocyte morphology and function become significantly altered in multiple neurodegenerative disorders, often referred to as astrocyte reactivity.[12–15]

Optic nerve head (ONH) astrocytes display biologic and morphologic reactivity to elevated IOP,[16–19] which is a risk factor in glaucomatous optic nerve axon degeneration.[20] Specifically, ONH astrocyte structural reactivity to elevated IOP includes alterations of cellular shape,[16] as well as orientation changes of cellular extensions that occur immediately after 8 hours of acute IOP elevation.[10,21] These structural changes are likely to include the actin cytoskeleton, as ONH astrocytes become more motile within 12 hours after exposure to increased hydrostatic pressure[22] and within 1 day after initiation of a wound healing assay[23] in vitro. Furthermore, ONH astrocytes exhibit enhanced phosphorylation of actin- and focal adhesion–based mediators (cortactin and paxillin, respectively) as early as 1-day post-elevated IOP in vivo.[21] This is consistent with rapid cortactin and paxillin phosphorylation in cultured tumor and stromal cells in response to stimuli.[24,25] In the setting of chronic IOP elevation in rats, 77 cytoskeletal genes were upregulated in early ONH injury (including cortactin gene expression, which was increased by 156% relative to controls).[26] In the same study, genes involved in cell motility were the fourth most upregulated DAVID gene ontology category in the early ONH injury group.[26] Proteomic analysis of nonhuman primate ONH tissue after chronic IOP elevation yielded several significantly upregulated actin cytoskeletal proteins relative to controls, including subunit 4 of actin related protein 2/3 (Arp 2/3) (Zhang L, et al. *IOVS* 2014;55:ARVO E-Abstract 4519), which is downstream of cortactin and involved in actin filament assembly.

ONH astrocyte reactivity is one of the earliest events in response to elevated IOP, and is often observed prior to any observable axon injury.[10,16,18,21,27] Thus, understanding the events leading to ONH astrocyte reactivity is critical to defining the role of astrocyte reactivity in glaucomatous axon degeneration.[17,28–30] ONH astrocyte reactivity may be initiated directly via primary local effects on astrocytes (including local biomechanical forces from IOP elevation),[31] or indirectly

through signaling and crosstalk between astrocytes and the axonal/extracellular environment at the site of injury. While astrocyte-axon communication and crosstalk has been well documented in several models,[32–34] the role of astrocyte-axon communication in initiating astrocyte reactivity remains an open question. Local elimination of axons prior to inducing astrocyte reactivity in a model is one way to address this question.

Here, using an adult rat model, we induced complete optic nerve axon loss by retrobulbar optic nerve transection (ONT). In addition, we used acute controlled elevation of IOP (CEI) to induce local ONH astrocyte reactivity.[21,35] We have shown previously that optic nerve axons exhibit minimal observable injury immediately after CEI (day 0 and day 1 post-IOP elevation),[21] while optic nerve axons exhibit essentially total degeneration 2 weeks post ONT as assessed by light microscopy.[10] Features of ONH astrocyte reactivity, including structural reorientation of astrocyte extensions and changes in label intensities of actin-, focal adhesion–, and complement-based mediators were studied in eyes after ONT alone, CEI alone, and combined ONT and CEI, and were compared with control eyes.

Materials and Methods

Animals

All animals were treated in accordance with the ARVO Statement for the Use of Animals in Ophthalmic and Vision Research[36] and all experimental methods were approved by the Oregon Health & Science University Institutional Animal Care and Use Committee. Animals underwent unilateral procedures only. Thirty-nine 8- to 9-month-old male Brown Norway rats (350–400 g) were randomized and underwent either unilateral retrobulbar ONT ($n = 8$), CEI ($n = 16$), or ONT followed by CEI 2 weeks post ONT ($n = 15$). Only male rats were used in this study. In prior experiments it proved difficult to consistently achieve a stable plane of anesthesia for the prolonged periods necessary in female rats, and mortality rates were unacceptable (data not shown).

Optic Nerve Transection (ONT)

For animals undergoing ONT ($n = 23$), rats received systemic anesthesia with intraperitoneal injection of ketamine (37.5 mg/kg; JHP Pharmaceuticals, Rochester, MI, USA), xylazine (7.5 mg/kg; RXV, Greeley, CO, USA), and acepromazine maleate (1.5 mg/kg; VET ONE, Boise, ID, USA). Topical 0.5% proparacaine hydrochloride ophthalmic solution (Akorn, Lake Forest, IL, USA) was applied to the ocular and conjunctival surface unilaterally. During anesthesia, animals remained on a temperature-controlled blanket at 37°C to maintain body temperature. The lateral canthus was clamped with a curved hemostatic Mosquito forceps, followed by a lateral canthotomy with Wescott scissors. A conjunctival peritomy was performed at the superior six clock hours of the limbus. The conjunctiva was retracted by an assistant to expose the superior rectus muscle insertion near the limbus. To gain access to the intraconal retrobulbar space, the superior rectus muscle was cauterized with low-temperature cautery (Bovie Medical, Clearwater, FL, USA) and transected with Vannas scissors. Care was taken to avoid injury to the superotemporal and superonasal vortex veins exiting the sclera. The eye was then inferoducted by grasping the remaining superior rectus muscle insertion using 0.12-mm toothed forceps. The junction of the superior optic nerve and the globe was exposed using a two-pronged instrument modified from a Lewis Lens Loop,[37] with care to avoid any trauma or excess stretch to the optic nerve. Next, a 25-G microvitreoretinal blade was used to carefully puncture the superior optic nerve sheath, as far away from the globe as possible. This was followed by dissection of the superior optic nerve sheath, using Vannas scissors. After adequate optic nerve sheath opening was confirmed, one arm of the Vannas scissors (with sharp edge oriented superiorly) was carefully placed between the optic nerve and the inferior optic nerve sheath, followed by total axonotomy as far posterior in the retrobulbar space as possible. The inferior optic nerve sheath and its vasculature was preserved without manipulation. The orbital contents and conjunctiva were carefully replaced in their original position, and the conjunctiva was re-approximated at the limbus using two interrupted 10-0 nylon sutures (Medtronic, Minneapolis, MN, USA). The periocular surface was cleaned and erythromycin ointment (Perrigo, Minneapolis, MN, USA) was applied to the ocular surface. Animals received postsurgical subcutaneous injections of 50 µL of 0.3 mg/mL buprenorphine (Buprenex; Reckitt Benckiser Pharmaceuticals, Richmond, VA, USA) for analgesia and were allowed to awaken from anesthesia on a warm platform. Animals were allowed to survive for 2 weeks prior to euthanization (ONT alone, $n = 8$) or CEI (combined ONT and CEI, see below).

Controlled Elevation of Intraocular Pressure (CEI)

Naïve animals ($n = 16$) or a portion of the animals which had undergone ONT 2 weeks prior ($n = 15$), underwent unilateral CEI as previously described.[21,35] Briefly, for IOP elevation, animals were maintained under general anesthesia using 2.25% isoflurane mixed with 100% oxygen, and kept at a temperature of 37°C using a water bath-heated temperature therapy pad. After topical 0.5% proparacaine application to the eye, a corneal incision was made using a 31-G needle with care to avoid iris or lens trauma. Next, the anterior chamber was cannulated through the corneal incision with a 2 cm length of 0.010" OD polyurethane tubing (Instech Labs, Plymouth Meeting, PA, USA) linked via larger tubing to a reservoir filled with pH-balanced saline solution (BSS Plus; Alcon Laboratories, Fort Worth, TX, USA). The saline reservoir was raised to produce a pressure of 60 mm Hg, as confirmed by a pressure sensor coupled with the infusion line (Harvard Apparatus, Holliston, MA, USA) and independent measurements every 30 minutes using a handheld tonometer (TonoLab; Icare Finland Oy, Espoo, Finland). Both eyes received topical proparacaine and topical BSS, alternating every 15 minutes to keep the ocular surface anesthetized and moist, respectively. Animals received a 1-mL subcutaneous injection of 0.9% saline every hour to maintain systemic hydration while under general anesthesia. After 8 hours of elevated IOP exposure, the saline reservoir was lowered to 20 mm Hg for 5 minutes, after which the cannula was removed and animals were sacrificed either immediately after IOP normalization (CEI day 0, $n = 8$ for CEI day 0 only, $n = 8$ for CEI day 0 + ONT), or allowed to survive for 1 day (CEI day 1, $n = 8$ for CEI day 1 only, $n = 7$ for CEI day 1 + ONT) prior to euthanization. For euthanization, animals were placed under deep sedation using 5% isoflurane anesthesia and underwent systemic perfusion-fixation via cardiac access with 1 L of buffered 4% paraformaldehyde over 20 minutes, as previously described.[38]

Axonal Injury Assessment

For axonal injury assessment, animals were euthanized under isoflurane anesthesia and eyes were perfusion-fixed with buffered 4% paraformaldehyde as described above. Eyes were enucleated and retrobulbar optic nerves 1 mm distal to the

Investigative Ophthalmology & Visual Science

globe were dissected. Retrobulbar nerves were postfixed in 5% glutaraldehyde for 24 hours, embedded in plastic, transversely sectioned, and stained with toluidine blue (Electron Microscopy Sciences, Hatfield, PA, USA), followed by light microscopy for assessment of morphologic evidence of axonal degeneration.[39]

Immunofluorescence Labeling of Optic Nerve Tissue

Perfusion-fixed eyes (including the ONH) were cryopreserved in 15% sucrose/PBS, followed by 30% sucrose/PBS. The eyes were positioned for vertical longitudinal sectioning centered on the optic nerve in 1:1 solution of optimal cutting temperature support medium (Sakura Finetek, Torrance, CA, USA) and 30% sucrose/PBS. Eyes were then frozen in liquid isopentane cooled by liquid nitrogen, and cryosectioned (5-μm thickness) onto glass slides. The superior and inferior orientation of the ONH was determined based on the anatomic location of the central retinal vein, located just inferior to the ONH.[40] Tissue sections were blocked with 1% bovine serum albumin (BSA) in PBS for 1 hour at room temperature. Actin filaments were labeled with 1 μg/mL tetramethylrhodamine (TRITC)-labeled phalloidin (Sigma, Sigma-Aldrich Corp., St. Louis, MO, USA) in 1% BSA/PBS at room temperature for 1 hour,[10,41] followed by three cycles of wash with PBS at room temperature for 5 minutes. Tissue sections were co-labeled with primary antibodies in 1% BSA/PBS at 4°C overnight, using antibodies against axonal tubulin (Tuj1; mouse monoclonal against βIII tubulin, 1:500 dilution; Covance, Seattle, WA, USA), phosphorylated paxillin (p-paxillin; rabbit polyclonal against phosphorylated Tyr 118, 1:100 dilution; Abcam, Cambridge, MA, USA), phosphorylated cortactin (p-cortactin; rabbit polyclonal against phosphorylated Tyr 421, 1:500 dilution; EMD Millipore, Billerica, MA, USA), or complement C3 (B-9 mouse monoclonal against amino acids 541-840 of human C3, 1:100 dilution; Santa Cruz Biotechnology, Dallas, TX, USA). Nonspecific mouse or rabbit IgG antibodies (Sigma) were used at similar concentrations to the respective antibodies above for negative control sections. Sections were washed as above, followed by incubation with secondary Alexa 488-labeled goat anti-mouse/rabbit monoclonal antibodies (ThermoFisher Scientific, Waltham, MA, USA) in 1% BSA/PBS for 1 hour at room temperature. After washing as above, cell nuclei were stained with the mounting media (Prolong Gold with DAPI; ThermoFisher Scientific). All immunofluorescent study *n*'s represent individual animals as biological replicates (i.e., 1 ONH section from each animal was labeled and analyzed for each *n*). A single section was chosen as close as possible to the center of the ONH from each animal, to improve anatomic consistency between samples. To reduce any potential labeling discrepancies within each antibody condition, each immunolabeling set (i.e., for filamentous actin plus either antitubulin, p-cortactin, p-paxillin, or complement C3) was completed in a single run. Primary antibodies used in label intensity measurements in this study were previously validated for specificity: antibodies against phosphorylated cortactin and phosphorylated paxillin were previously validated in our lab,[21] while the specificity of the antibody against complement C3 has been established by the manufacturer (www.scbt.com/scbt/product/c3-antibody-b-9, in the public domain) using recombinant expression for validation.[42]

Confocal Microscopy and Image Analysis

All slides were labeled with a unique four-digit number. Random samples for each antibody label were briefly used to adjust the saturation and background intensities of the samples under confocal microscopy and camera settings (FV1000 microscope; Olympus, Center Valley, PA, USA; and an UplanFLN ×40/NA1.30 oil objective; Olympus) to be within the linear range of the camera and avoid over/undersaturation. These settings were then applied to all samples going forward to maintain consistent imaging. We have previously shown that ONH astrocyte extension rearrangement in response to CEI was more significant in the inferior ONH, relative to the superior ONH.[21] In this study, we confirmed that the inferior ONH indeed showed more astrocyte extension rearrangement in response to CEI, relative to the superior ONH (data not shown). Thus, we present data from the inferior ONH in this study.

Confocal images of the inferior ONH (the anterior and posterior borders defined as 0 and 100 μm posterior to the termination of Bruch's membrane, respectively) were obtained. Images were captured using FV10-ASW version 4.0 software (Olympus) with laser wavelength settings of 405, 488, and 559 nm at 1 μm/slice. Confocal microscopy image acquisition was performed in the same manner on all slides within an antibody condition (including the same laser settings, magnification, exposure time, intensity range, and image capture size). Captured images were imported directly into FIJI image analysis software (http://fiji.sc/Fiji; an open source image processing package based on the National Institute of Health, Bethesda, Maryland, USA software ImageJ: http://imagej.nih.gov/ij/), and were analyzed as Z-stacks in a semiautomated fashion (including analyzing the entire Z-stack image at once without user manipulation, and using the same analysis settings for all images). ONH actin bundle orientation was determined using the Directionality plug-in in FIJI as previously described.[21] Mean fluorescence pixel intensities for phosphorylated cortactin, phosphorylated paxillin, and complement C3 were calculated using FIJI software. Upon completion of image acquisition and analysis, the key for identifying which sample/data belonged to which treatment group was then used to group the samples. Statistical analysis was performed by 1- or 2-way ANOVA (GraphPad Prism software, La Jolla, CA, USA), followed by Sidak's and/or Dunnett's multiple comparisons testing. Data were log transformed when necessary to meet the assumption of normal variance prior to ANOVA analysis. All data generated or analyzed during this study are included in this published article.

Results

Axon Degeneration Following IOP Elevation and Optic Nerve Transection

We confirmed that optic nerves of animals undergoing CEI exhibited no observable axon injury immediately following CEI relative to controls (Figs. 1A, 1B, 1D, 1E). In contrast, 2 weeks after ONT, optic nerves exhibited essentially total axon degeneration (Figs. 1C, 1F).

IOP Elevation Induces Similar Astrocyte Structural Remodeling in the Presence or Absence of Viable Optic Nerve Axons

In order to assess the structural response of ONH astrocytes to IOP elevation in the presence or absence of viable axons, we quantified the orientation of astrocyte extensions within the ONH. The ONH is rich in astrocytic actin filaments (Fig. 2A) that delineate astrocyte extensions, with high concordance with astrocyte-specific markers such as glial fibrillary acidic protein (GFAP) and aquaporin 4.[10] As previously reported,[10,21,37] control ONH astrocytes exhibit highly arranged,

Investigative Ophthalmology & Visual Science

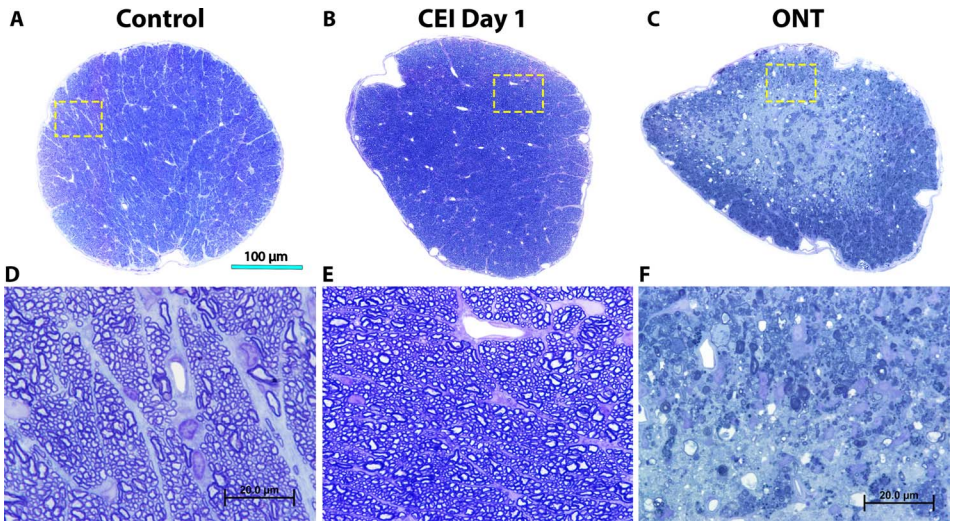

FIGURE 1. Optic nerve axonal appearance after CEI or ONT. Transverse sections of retrobulbar optic nerves stained with toluidine blue. Representative low magnification images of a control optic nerve (**A**), as well as optic nerves 1 day post CEI (**B**), or 2 weeks post ONT (**C**). High-magnification images of optic nerves (**D**–**F**) corresponding to insets (*yellow box*) from the low-magnification images (**A**–**C**). Note the highly organized and intact axons and axon bundles in control (**A**, **D**) and CEI day 1 (**B**, **E**) nerves, in contrast to significant axon degeneration noted after ONT (**C**, **F**).

actin-based extensions perpendicular (84.3° ± 1.0°) to the anterior-posterior and axonal microtubule axes (Fig. 2B, top row; Fig. 2D). However, immediately after IOP elevation (CEI day 0), astrocyte extensions become less organized with an orientation less perpendicular (62.2° ± 7.3°, $P < 0.01$ relative to controls) to the axonal axis (Fig. 2B, middle row; Fig. 2D). One day after IOP normalization (CEI day 1), ONH astrocyte extensions rearranged back to the orientation (83.9° ± 1.8°) observed in controls (Fig. 2B, bottom row; Fig. 2D).

In eyes that underwent ONT only, astrocyte extensions remained essentially unaltered and maintained their overall perpendicular axis (72.8° ± 4.8°) relative to the anterior-posterior axis (Fig. 2C, top row; Fig. 2D). As expected, no observable axonal tubulin labeling was detected in the ONH post-ONT, due to global axon degeneration (Fig. 2C). In eyes that underwent CEI post-ONT, ONH astrocyte extensions became highly disorganized and significantly rearranged (65.2° ± 6.6° relative to the anterior-posterior axis, $P < 0.01$ relative to controls) immediately after IOP elevation (CEI day 0 + ONT), in a similar fashion to CEI day 0 alone, despite the lack of any observable axons (Fig. 2C, middle row; Fig. 2D). Also, as seen in CEI day 1 alone, ONH astrocyte extensions rearranged back to control orientation (81.6° ± 2.6° relative to the anterior-posterior axis) 1 day after CEI post-ONT (CEI day 1 + ONT), despite the lack of any observable optic nerve axons (Fig. 2C, bottom row; Fig. 2D). This structural response of astrocyte extensions to CEI was quantified, and showed a statistically significant reduction in the orientation of astrocyte extensions immediately after IOP elevation, both in the presence or absence of viable axons (Fig. 2D). In addition, 1 day post CEI, astrocyte extensions re-oriented back the orientation level observed in control ONHs, in the presence or absence of viable axons (Fig. 2D).

Astrocytes Display Differential Phosphorylation of Cytoskeletal Mediators in Response to Elevated IOP in the Presence or Absence of Viable Optic Nerve Axons

We have previously shown that the phosphorylation status of actin cytoskeletal and focal adhesion mediators within ONH astrocytes are significantly altered immediately after IOP elevation.[21] Here, we asked if the phosphorylation status of ONH cortactin (involved in dynamic actin turnover)[41,43] and paxillin (involved in focal adhesion dynamics)[44,45] in response to IOP elevation, was affected by the presence or absence of viable axons.

Control ONHs displayed low label intensity (62.5 ± 5.3 arbitrary units [AU]) for phosphorylated cortactin, which remained low (38.5 ± 4.1 AU) immediately after IOP elevation (CEI day 0), but became significantly elevated (87.0 ± 12.3 AU, $P < 0.005$) 1 day after IOP elevation (CEI day 1 versus CEI day 0; Fig. 3A, 3B). However, IOP elevation in the setting of ONT (CEI day 0 + ONT, and CEI day 1 + ONT) resulted in significantly lower phosphorylated cortactin label intensity (60.7 ± 8.8 and 47.2 ± 6.6 AU, respectively) relative to ONT alone (95.1 ± 6.6 AU, $P < 0.05$; Figs. 3A, 3B). By 1 day post CEI, phosphorylated cortactin label intensities within the ONH with intact axons were significantly higher compared with values in the absence of viable axons (87.0 ± 12.3 vs. 47.2 ± 6.6 AU, $P < 0.05$; Figs. 3A, 3B).

Control ONHs displayed low phosphorylated paxillin label intensity (23.4 ± 1.8 AU), which significantly increased 1 day after CEI alone (32.9 ± 2.4 AU, $P < 0.05$), relative to controls (Figs. 4A, 4B). ONT alone significantly increased ONH phosphorylated paxillin label intensity (34.2 ± 2.3 AU) relative to control (24.1 ± 1.6 AU) and CEI day 0 alone ($P < 0.05$; Figs. 4A, 4B). However, when CEI and ONT were combined, ONH phosphorylated paxillin label intensities (27.6 ± 1.6 AU for CEI day 0 + ONT; 30.1 ± 3.5 AU for CEI day 1 + ONT) were not significantly different than controls (Figs. 4A, 4B). Both immediately after CEI (CEI day 0) and 1 day post CEI (CEI day 1), phosphorylated paxillin label intensities within the ONH were similar in the presence or absence of viable axons (Figs. 4A, 4B).

Astrocytic Complement C3 Label Intensities are Unaffected by Acute IOP Elevation or Optic Nerve Transection

The complement cascade has been implicated in astrocyte reactivity,[46] and elevated levels of complement C3 mRNA and

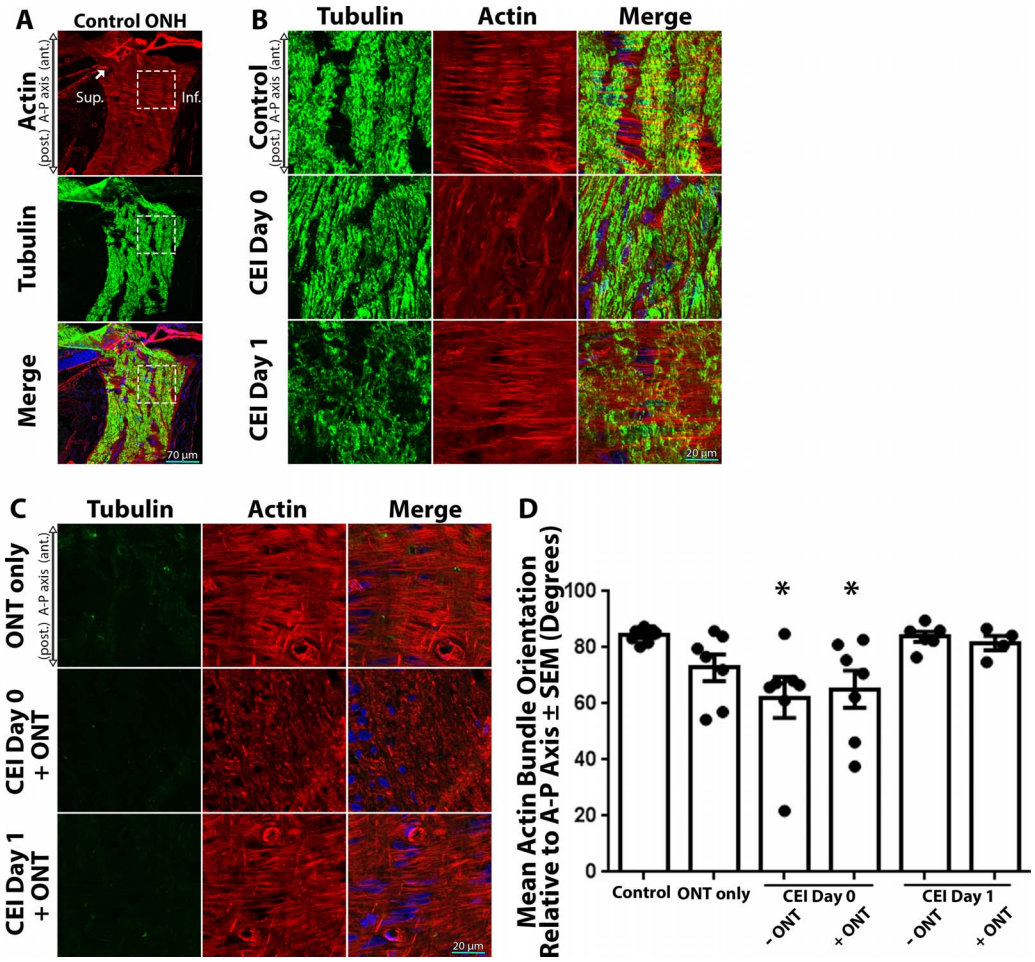

Figure 2. Actin-based astrocyte extensions change orientation within hours after IOP elevation, in the presence or absence of viable axons. (**A**) Low-magnification images of the ONH and surrounding tissue labeled for actin filaments (*red*, TRITC-phalloidin), axonal tubulin (*green*, Tuj1 anti-tubulin βIII antibody), and nuclei (*blue*, DAPI). Superior (Sup.) and inferior (Inf.) anatomic locations are identified for orientation. The *dashed box* indicates the inferior ONH magnified in the *top panel* of (**B**). The *arrow* indicates the termination of Bruch's membrane (**B**, **C**) High-magnification images of the inferior ONH labeled for axonal tubulin, actin filaments, and nuclei. (**B**) Control ONH astrocytes display highly ordered actin-rich extensions, which are oriented perpendicular to the axonal and anterior (ant.)-posterior (post.) or A-P axis (*top row*). Immediately after CEI (Day 0), astrocyte extensions become disoriented relative to controls (*middle row*). Astrocyte extension reorient back to baseline orientation 1-day post-IOP normalization (CEI day 1; *bottom row*). (**C**) Two weeks post ONT, ONH axon tubulin labeling is essentially eliminated due to global optic nerve axon degeneration. However, ONH astrocyte extension maintain their orientation (*top row*) relative to controls (**B**, *top row*), despite total loss of axons. In post-ONT eyes, astrocyte extensions become immediately disoriented after CEI (**C**, CEI day 0 + ONT) relative to controls. Even post ONT, ONH astrocyte extensions reorient back to baseline orientation 1-day post-IOP normalization (**C**, CEI day 1 + ONT). (**D**) Mean astrocytic actin bundle orientation relative to the A-P axis within the ONH of control eyes and eyes exposed to ONT only, CEI only, or combined CEI + ONT. *Error bars* indicate standard error of the mean (SEM); $^*P < 0.05$ and indicates a statistically significant difference between control and experimental groups; $n = 7$, 7, 7, 7, 6, and 4 for each *column* from *left* to *right*, and represents individual animals.

protein have been observed in an optic nerve crush model[47] and a genetic glaucoma model,[48] respectively. We asked if complement C3 label intensities were altered in response to acute IOP elevation, in the presence or absence of viable axons. Control ONHs displayed moderate label intensity of complement C3 (37.4 ± 3.3 AU), which were not significantly altered immediately (33.2 ± 2.3 AU) or 1 day (43.5± 2.9 AU) after CEI alone (Figs. 5A, 5B). Similarly, ONH complement C3 label intensity was unaltered after ONT alone (35.8 ± 4.1 AU), relative to controls (Figs. 5A, 5B). The combination of CEI and ONT did not show any significant change in complement C3 label intensity within the ONH relative to controls (36.7 ± 2.2 AU for CEI day 0 + ONT; 31.4 ± 4.2 AU for CEI day 1 + ONT; Figs. 5A, 5B). Thus, complement C3 label intensities within the ONH appear to be unchanged after acute IOP elevation, ONT, or combined IOP elevation and ONT.

Discussion

Astrocyte reactivity is observed in multiple neurodegenerative disorders and blocking astrocyte reactivity reduces axon injury.[46] In glaucoma models with elevated IOP, ONH astrocyte reactivity occurs prior to observable axon injury.[10,21,28,49] However, it remains unclear if in vivo ONH astrocyte reactivity is initiated de novo in direct response to the glaucomatous insult (including biomechanical injury to the ONH),[29,50] or if astrocyte reactivity is initiated in response to ONH axonal, extracellular, or microglial[47,51,52] cues. Here, using a well-established model of acute IOP elevation (which leads to ONH astrocyte reactivity), in combination with ONT (which leads to nearly total loss of axon viability), we show that ONH astrocyte reactivity displays both axon-dependent and -independent features.

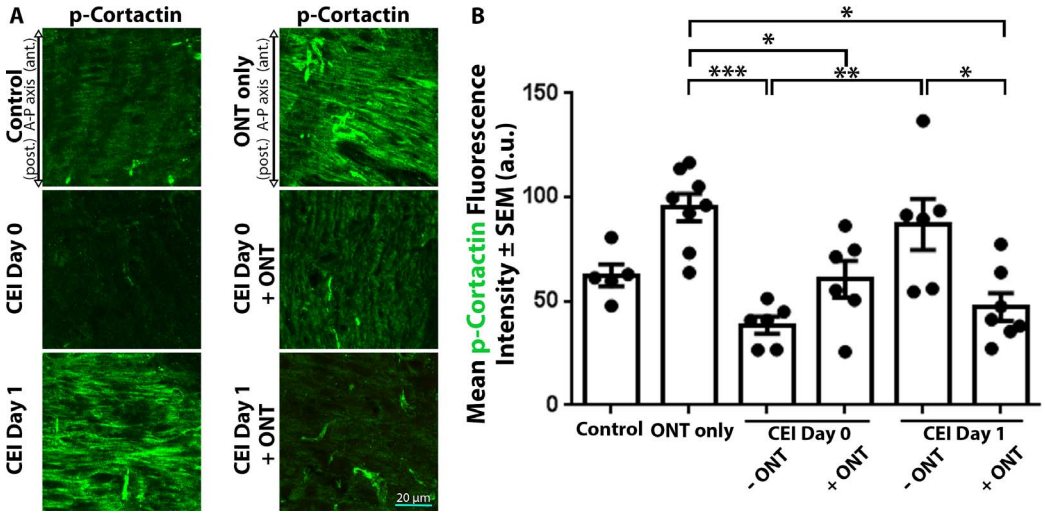

Figure 3. ONH cortactin phosphorylation label intensities respond differentially after IOP elevation, in the presence or absence of viable axons. (**A**) ONH sections labeled with antiphosphorylated cortactin (p-cortactin) antibodies in control eyes and eyes exposed to CEI, ONT, or a combination of CEI + ONT. ONH p-cortactin label intensity significantly increased 1 day post CEI (**A**, **B**, CEI day 1 versus CEI day 0). However, when CEI and ONT were combined, ONH p-cortactin label intensity significantly decreased after CEI (**A**, **B**). (**B**) Mean p-cortactin label intensities within the ONH of control eyes and eyes exposed to ONT only, CEI only, or combined CEI + ONT. *Error bars* indicate SEM; $^{*}P < 0.05$, $^{**}P < 0.005$, and $^{***}P < 0.0001$ and indicates statistical significance; $n = 5$, 8, 6, 6, 6, and 7 for each *column* from *left* to *right*, and represents individual animals.

Our results show that structural ONH astrocyte responses to elevated IOP (namely the re-orientation of astrocyte extensions) occurs despite the total loss of axons, in a similar fashion to ONHs with intact axons. Thus, some ONH astrocyte structural responses to elevated IOP appear to be independent of viable axons, and do not depend on yet unidentified axon signaling. This is supported by three-dimensional astrocyte culture models in which deformations of the culture matrix cause re-orientation of astrocyte, despite the absence of neurons/axons in the culture model.[31] In addition, cultured ONH astrocytes in the absence of neurons display significant actin-based motility within 1 day after initiation of a wound healing assay,[23] and become four to six times more motile 12 hours after exposure to elevated hydrostatic pressure in vitro.[22] ONH astrocyte reactivity to IOP elevation may lead to local remodeling of the extracellular matrix and glial architecture that results in glaucomatous optic disc features seen clinically.[53] However, additional studies in models of ONH remodeling that include a collagenous lamina cribrosa and lamina cribrosa cells (which are not present in the rodent ONH), as well as consideration of other mechanistic factors, such as vascular insufficiency,[54,55] reduced metabolic support for axons,[56] neuroinflammation,[57] and the contribution of microglia[47,51,52] may shed further light on the pathophysiology of ONH remodeling and axon injury in human glaucoma.

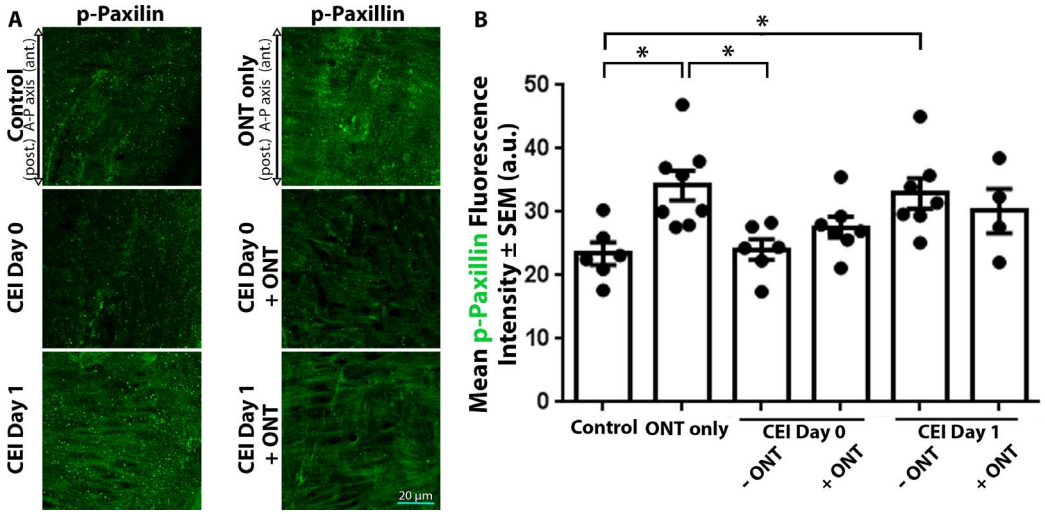

Figure 4. Paxillin phosphorylation label intensities within the ONH increase after ONT, but not when combined with IOP elevation. (**A**) ONH sections labeled with antiphosphorylated paxillin (p-paxillin) antibodies in control eyes and eyes exposed to CEI, ONT, or a combination of CEI and ONT. ONH p-paxillin label intensity significantly increased 1 day after CEI alone, relative to controls (**A**, **B**). However, when CEI and ONT were combined, ONH p-paxillin label intensity did not significantly change relative to controls or CEI alone (**A**, **B**). (**B**) Mean p-paxillin label intensities within the ONH of control eyes and eyes exposed to ONT only, CEI only, or combined CEI + ONT. *Error bars* indicate SEM; $^{*}P < 0.05$ and indicates statistical significance; $n = 6$, 8, 6, 7, 7, and 4 for each *column* from *left* to *right*, and represents individual animals.

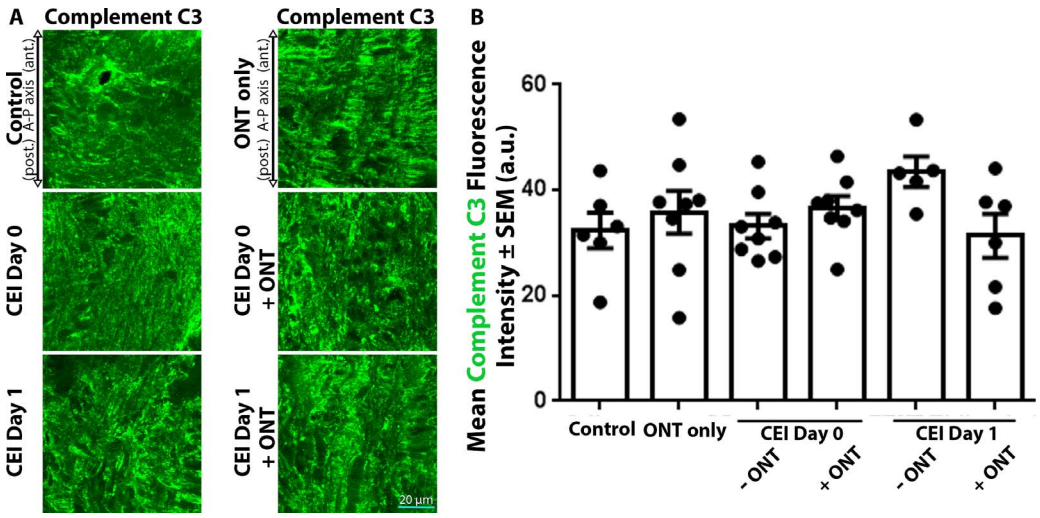

Figure 5. Complete C3 label intensities within the ONH remain unchanged after CEI, ONT, or combined CEI and ONT. (**A**) ONH sections labeled with anticomplement C3 antibodies in control eyes and eyes exposed to CEI, ONT, or a combination of CEI and ONT. (**A**) ONH complement C3 label intensities remain unchanged in all experimental groups, relative to controls. (**B**) Mean complement C3 label intensities within the ONH of control eyes and eyes exposed to ONT only, CEI only, or combined CEI + ONT. *Error bars* indicate SEM. No statistical significance between groups was noted using ANOVA analysis; $n = 6, 8, 8, 8, 5$, and 6 for each *column* from *left* to *right* and represents individual animals.

Despite our findings that ONT does not affect the structural response of astrocytes to CEI, we show evidence that certain molecular ONH astrocyte responses to elevated IOP display axon-dependent features. For example, phosphorylation of ONH cortactin (which is a substrate for Src kinase and activates Arp2/3 complex leading to increased actin filament formation)[41,43] is significantly increased between day 0 and day 1 after IOP elevation. Cortactin phosphorylation enhances actin polymerization through Arp 2/3 activation and is necessary for rapid actin cytoskeletal turnover,[43] particularly in the leading edge of motile cells and protruding cellular extensions.[58] The significantly increased label intensity of phosphorylated cortactin within the ONH 1 day after IOP normalization is likely involved in astrocyte extension re-formation and re-orientation back to baseline levels. This is consistent with astrocyte structural changes observed in models with randomly labeled astrocytes within the ONH, which show that acute IOP elevation leads to extension retraction, followed extension reformation once IOP is normalized.[18] In this study, when IOP elevation was performed in the absence of viable axons, ONH phosphorylated cortactin label intensities significantly decreased after IOP elevation. This suggests other astrocyte actin cytoskeletal activation pathways may be involved in the re-alignment of astrocyte extensions post-IOP normalization in the absence of viable axons (possibly via enhanced astrocyte interactions with extracellular matrix[59] or microglia[60,61] in the absence of axons). Additionally, cortactin is a substrate for multiple kinases (including Src, Fer, FAK, and ERK1/2)[24,62–64] and is phosphorylated on multiple tyrosine and serine sites,[24,65] which may lead to variable astrocytic cortactin phosphorylation and activation depending on which upstream kinases are activated in the presence or absence of axons.

Astrocyte focal adhesion-based response through paxillin phosphorylation (which is a substrate for the Src-FAK complex and a major component of focal adhesions[45]), was significantly elevated 1 day after IOP elevation alone relative to controls. This may be consistent with enhanced astrocyte cellular extension formation within the ONH after IOP normalization, as focal adhesion molecules and signaling are important regulators of astrocyte morphology in a *Drosophila* model.[66] ONT alone also resulted in a significantly higher label intensity of astrocytic paxillin phosphorylation within the ONH relative to controls, potentially due to enhanced astrocyte-extracellular matrix interactions as seen in a two-dimensional culture model of astrocytes without axons.[59] However, the increase in phosphorylated paxillin label intensity post ONT relatively to controls was not seen when ONT was combined with CEI. This may imply that astrocyte-axon interactions may be necessary for optimal focal adhesion formation within the ONH post-IOP normalization. Thus, there are likely intimate links between astrocyte actin/focal adhesion mediators and axons, which may be facilitated through axonal crosstalk and regulation. This may be expected given the intimate physical relationship of astrocyte extensions, axon bundles, and the complex extracellular matrix of the ONH (Johnson EC, et al. *IOVS* 1994:ARVO Abstract 1850).[67]

While we note that structural, actin-based responses of ONH astrocytes to elevated IOP (namely extension orientation) are unchanged in the absence of axons, we also noted that some of the actin- and focal adhesion–based phosphorylation events in response to elevated IOP are dependent on the presence of viable axons. In addition to large structural astrocyte orientation changes, there are likely ultrastructural actin-based changes occurring within ONH astrocytes in the setting of IOP elevation (including changes in actin bundle thickness, length, and/or turnover rate),[68] that we simply cannot quantify in a tissue section of densely interdigitated astrocytes. In a mouse model expressing green fluorescent protein in random individual astrocytes, Wang et al.[16] have shown that after IOP elevation ONH astrocytes display new, relatively short cellular extensions along the longitudinal axis of the optic nerve that invade axon bundles of the ONH. Many of these finer ultrastructural changes may involve changes in phosphorylation levels of cortactin[65,69] and paxillin,[44,45] which we do see in our model. Thus, astrocyte-axon crosstalk may be an important component of overall astrocytic response to elevated IOP within the ONH.

Complement C3 is central to both classical and alternative pathways of complement activation. Within the ONH, complement C3 gene expression increases in various models of chronic IOP elevation, including the genetic DBA/2J mouse model[48] and a laser model of IOP elevation.[70] However, in a

chronic model of IOP elevation in rats using episcleral hypertonic saline injection, Johnson et al.[26] found that ONH complement C3 gene expression was not significantly elevated with either early or advanced injury. Within the optic nerve, Ohlsson et al.[47] observed significantly elevated message levels of complement C3 distal to the site of optic nerve crush. Kuehn et al.[70] noted increased complement C3 gene expression and protein levels within the nerve fiber and ganglion cell layers of the retina (but not the ONH) in mice that underwent laser-induced IOP elevation. In our study, we found no significant changes in complement C3 label intensity within the ONH after IOP elevation, ONT, or their combination. The discrepancy between some of these results in various models may be due to the different length and degree of IOP elevation between models. The lack of changes in complement C3 label intensity within the ONH in our model further highlights the specificity of the other changes noted (namely the structural and actin/focal adhesion–mediator reactivity described above).

Our results support astrocyte reactivity as a possible link between the initial biomechanical insult to the ONH after IOP elevation,[28,50] and eventual axon degeneration. Early axon-dependent or -independent structural and molecular astrocyte reactivity may reduce the ability of astrocytes to provide mechanical and metabolic support for axons. Indeed, reactive astrocytes lose the ability to promote neuronal survival in culture.[46] Taken together, these results favor a model in which astrocytes are the primary and earliest sensors of ONH injury in glaucoma, and their response to injury precedes and may lead to eventual axon degeneration in glaucoma. Future studies in other model paradigms will help overcome some of the limitations of this study, including the relatively short time course of IOP elevation and follow-up time period, as well as the lack of a true lamina cribrosa in the rodent ONH. Additionally, gene expression studies and proteomic analysis within the ONH may shed further light on the additional cellular and molecular pathways involved in astrocyte reactivity to elevation IOP.

Acknowledgments

The authors thank Bang Bui (University of Melbourne, Australia) for helpful discussion of the results.

Supported by grants from Research to Prevent Blindness (New York, NY, USA: Career Development Award to ST and unrestricted grant to OHSU), and the National Institutes of Health (Bethesda, MD, USA: K08EY024025 to ST, R01EY010145 to JCM, and P30EY010572 to OHSU).

Disclosure: **S. Tehrani**, None; **L. Davis**, None; **W.O. Cepurna**, None; **R.K. Delf**, None; **D.C. Lozano**, None; **T.E. Choe**, None; **E.C. Johnson**, None; **J.C. Morrison**, None

References

1. Davis CH, Kim KY, Bushong EA, et al. Transcellular degradation of axonal mitochondria. *Proc Natl Acad Sci U S A*. 2014;111:9633–9638.
2. Lundgaard I, Osorio MJ, Kress BT, Sanggaard S, Nedergaard M. White matter astrocytes in health and disease. *Neuroscience*. 2014;276:161–173.
3. Jones EV, Bouvier DS. Astrocyte-secreted matricellular proteins in CNS remodelling during development and disease. *Neural plasticity*. 2014;2014:321209.
4. Edgar JM, Nave KA. The role of CNS glia in preserving axon function. *Curr Opin Neurobiol*. 2009;19:498–504.
5. Pellerin L, Bouzier-Sore AK, Aubert A, et al. Activity-dependent regulation of energy metabolism by astrocytes: an update. *Glia*. 2007;55:1251–1262.
6. Ransom B, Behar T, Nedergaard M. New roles for astrocytes (stars at last). *Trends Neurosci*. 2003;26:520–522.
7. Gimenez y Ribotta M, Menet V, Privat A. The role of astrocytes in axonal regeneration in the mammalian CNS. *Prog Brain Res*. 2001;132:587–610.
8. Coles JA, Vega C, Marcaggi P. Metabolic trafficking between cells in nervous tissue. *Prog Brain Res*. 2000;125:241–254.
9. Butt AM, Colquhoun K, Berry M. Confocal imaging of glial cells in the intact rat optic nerve. *Glia*. 1994;10:315–322.
10. Tehrani S, Johnson EC, Cepurna WO, Morrison JC. Astrocyte processes label for filamentous actin and reorient early within the optic nerve head in a rat glaucoma model. *Invest Ophthalmol Vis Sci*. 2014;55:6945–6952.
11. Sun D, Lye-Barthel M, Masland RH, Jakobs TC. The morphology and spatial arrangement of astrocytes in the optic nerve head of the mouse. *J Comp Neurol*. 2009;516:1–19.
12. Chun H, Lee CJ. Reactive astrocytes in Alzheimer's disease: a double-edged sword. *Neurosci Res*. 2018;126:44–52.
13. Adams KL, Gallo V. The diversity and disparity of the glial scar. *Nat Neurosci*. 2018;21:9–15.
14. Sun D, Jakobs TC. Structural remodeling of astrocytes in the injured CNS. *Neuroscientist*. 2012;18:567–588.
15. Pekny M, Nilsson M. Astrocyte activation and reactive gliosis. *Glia*. 2005;50:427–434.
16. Wang R, Seifert P, Jakobs TC. Astrocytes in the optic nerve head of glaucomatous mice display a characteristic reactive phenotype. *Invest Ophthalmol Vis Sci*. 2017;58:924–932.
17. Tamm ER, Ethier CR; for the Lasker/IRRF Initiative on Astrocytes and Glaucomatous Neurodegeneration Participants. Biological aspects of axonal damage in glaucoma: a brief review. *Exp Eye Res*. 2017;157:5–12.
18. Sun D, Qu J, Jakobs TC. Reversible reactivity by optic nerve astrocytes. *Glia*. 2013;61:1218–1235.
19. Qu J, Jakobs TC. The time course of gene expression during reactive gliosis in the optic nerve. *PLoS One*. 2013;8:e67094.
20. Burgoyne CF, Downs JC, Bellezza AJ, Suh JK, Hart RT. The optic nerve head as a biomechanical structure: a new paradigm for understanding the role of IOP-related stress and strain in the pathophysiology of glaucomatous optic nerve head damage. *Prog Retin Eye Res*. 2005;24:39–73.
21. Tehrani S, Davis L, Cepurna WO, et al. Astrocyte structural and molecular response to elevated intraocular pressure occurs rapidly and precedes axonal tubulin rearrangement within the optic nerve head in a rat model. *PLoS One*. 2016;11:e0167364.
22. Tezel G, Hernandez MR, Wax MB. In vitro evaluation of reactive astrocyte migration, a component of tissue remodeling in glaucomatous optic nerve head. *Glia*. 2001;34:178–189.
23. Salvador-Silva M, Aoi S, Parker A, Yang P, Pecen P, Hernandez MR. Responses and signaling pathways in human optic nerve head astrocytes exposed to hydrostatic pressure in vitro. *Glia*. 2004;45:364–377.
24. Kelley LC, Hayes KE, Ammer AG, Martin KH, Weed SA. Cortactin phosphorylated by ERK1/2 localizes to sites of dynamic actin regulation and is required for carcinoma lamellipodia persistence. *PLoS One*. 2010;5:e13847.
25. Jarvis LJ, Maguire JE, LeBien TW. Contact between human bone marrow stromal cells and B lymphocytes enhances very late antigen-4/vascular cell adhesion molecule-1-independent tyrosine phosphorylation of focal adhesion kinase, paxillin, and ERK2 in stromal cells. *Blood*. 1997;90:1626–1635.
26. Johnson EC, Doser TA, Cepurna WO, et al. Cell proliferation and interleukin-6-type cytokine signaling are implicated by gene expression responses in early optic nerve head injury in rat glaucoma. *Invest Ophthalmol Vis Sci*. 2011;52:504–518.

27. Cooper ML, Collyer JW, Calkins DJ. Astrocyte remodeling without gliosis precedes optic nerve axonopathy. *Acta Neuropathol Commun*. 2018;6:38.
28. Stowell C, Burgoyne C, Tamm ER, Ethier CR; for the Lasker/IRRF Initiative on Astrocytes and Glaucomatous Neurodegeneration Participants. Biomechanical aspects of axonal damage in glaucoma: a brief review. *Exp Eye Res*. 2017;157:13–19.
29. Lukovic D, Stojkovic M, Moreno-Manzano V, et al. Concise review: reactive astrocytes and stem cells in spinal cord injury: good guys or bad guys? *Stem Cells*. 2015;33:1036–1041.
30. Johnson EC, Morrison JC. Friend or foe? Resolving the impact of glial responses in glaucoma. *J Glaucoma*. 2009;18:341–353.
31. Mulvihill JJE, Raykin J, Snider EJ, et al. Development of a platform for studying 3D astrocyte mechanobiology: compression of astrocytes in collagen gels. *Ann Biomed Eng*. 2017;46:365–374.
32. Gomez-Gonzalo M, Martin-Fernandez M, Martinez-Murillo R, et al. Neuron-astrocyte signaling is preserved in the aging brain. *Glia*. 2017;65:569–580.
33. Poskanzer KE, Yuste R. Astrocytes regulate cortical state switching in vivo. *Proc Natl Acad Sci U S A*. 2016;113:E2675–E2684.
34. Ma Z, Stork T, Bergles DE, Freeman MR. Neuromodulators signal through astrocytes to alter neural circuit activity and behaviour. *Nature*. 2016;539:428–432.
35. Morrison JC, Cepurna WO, Tehrani S, et al. A period of controlled elevation of IOP (CEI) produces the specific gene expression responses and focal injury pattern of experimental rat glaucoma. *Invest Ophthalmol Vis Sci*. 2016;57:6700–6711.
36. Association for Research in Vision and Ophthalmology. Statement for the Use of Animals in Ophthalmic and Visual Research; 2016. Available at http://www.arvo.org/About_ARVO/Policies/Statement_for_the_Use_of_Animals_in_Ophthalmic_and_Visual_Research/.
37. Tehrani S, Delf RK, Cepurna WO, Davis L, Johnson EC, Morrison JC. In vivo small molecule delivery to the optic nerve in a rodent model. *Sci Rep*. 2018;8:4453.
38. Morrison JC, Moore CG, Deppmeier LM, Gold BG, Meshul CK, Johnson EC. A rat model of chronic pressure-induced optic nerve damage. *Exp Eye Res*. 1997;64:85–96.
39. Jia L, Cepurna WO, Johnson EC, Morrison JC. Patterns of intraocular pressure elevation after aqueous humor outflow obstruction in rats. *Invest Ophthalmol Vis Sci*. 2000;41:1380–1385.
40. Pazos M, Yang H, Gardiner SK, et al. Rat optic nerve head anatomy within 3D histomorphometric reconstructions of normal control eyes. *Exp Eye Res*. 2015;139:1–12.
41. Tehrani S, Faccio R, Chandrasekar I, Ross FP, Cooper JA. Cortactin has an essential and specific role in osteoclast actin assembly. *Mol Biol Cell*. 2006;17:2882–2895.
42. Edfors F, Hober A, Linderback K, et al. Enhanced validation of antibodies for research applications. *Nat Commun*. 2018;9:4130.
43. Tehrani S, Tomasevic N, Weed S, Sakowicz R, Cooper JA. Src phosphorylation of cortactin enhances actin assembly. *Proc Natl Acad Sci U S A*. 2007;104:11933–11938.
44. Romanova LY, Mushinski JF. Central role of paxillin phosphorylation in regulation of LFA-1 integrins activity and lymphocyte migration. *Cell Adh Migr*. 2011;5:457–462.
45. Webb DJ, Donais K, Whitmore LA, et al. FAK-Src signalling through paxillin, ERK and MLCK regulates adhesion disassembly. *Nat Cell Biol*. 2004;6:154–161.
46. Liddelow SA, Guttenplan KA, Clarke LE, et al. Neurotoxic reactive astrocytes are induced by activated microglia. *Nature*. 2017;541:481–487.
47. Ohlsson M, Bellander BM, Langmoen IA, Svensson M. Complement activation following optic nerve crush in the adult rat. *J Neurotrauma*. 2003;20:895–904.
48. Harder JM, Braine CE, Williams PA, et al. Early immune responses are independent of RGC dysfunction in glaucoma with complement component C3 being protective. *Proc Natl Acad Sci U S A*. 2017;114:E3839–E3848.
49. Sun D, Moore S, Jakobs TC. Optic nerve astrocyte reactivity protects function in experimental glaucoma and other nerve injuries. *J Exp Med*. 2017;214:1411–1430.
50. Burgoyne CF. A biomechanical paradigm for axonal insult within the optic nerve head in aging and glaucoma. *Exp Eye Res*. 2010;93:120–132.
51. Bordone MP, Gonzalez Fleitas MF, Pasquini LA, et al. Involvement of microglia in early axoglial alterations of the optic nerve induced by experimental glaucoma. *J Neurochem*. 2017;142:323–337.
52. Gallego BI, Salazar JJ, de Hoz R, et al. IOP induces upregulation of GFAP and MHC-II and microglia reactivity in mice retina contralateral to experimental glaucoma. *J Neuroinflammation*. 2012;9:92.
53. Lee EJ, Han JC, Kee C. A novel hypothesis for the pathogenesis of glaucomatous disc hemorrhage. *Prog Retin Eye Res*. 2017;60:20–43.
54. Osborne NN, Melena J, Chidlow G, Wood JP. A hypothesis to explain ganglion cell death caused by vascular insults at the optic nerve head: possible implication for the treatment of glaucoma. *Br J Ophthalmol*. 2001;85:1252–1259.
55. Yamamoto T, Kitazawa Y. Vascular pathogenesis of normal-tension glaucoma: a possible pathogenetic factor, other than intraocular pressure, of glaucomatous optic neuropathy. *Prog Retin Eye Res*. 1998;17:127–143.
56. Inman DM, Harun-Or-Rashid M. Metabolic vulnerability in the neurodegenerative disease glaucoma. *Front Neurosci*. 2017;11:146.
57. Williams PA, Marsh-Armstrong N, Howell GR; for the Lasker/IRRF Initiative on Astrocytes and Glaucomatous Neurodegeneration Participants. Neuroinflammation in glaucoma: a new opportunity. *Exp Eye Res* 2017;157:20–27.
58. Huang C, Liu J, Haudenschild CC, Zhan X. The role of tyrosine phosphorylation of cortactin in the locomotion of endothelial cells. *J Biol Chem*. 1998;273:25770–25776.
59. Sato J, Horibe S, Kawauchi S, Sasaki N, Hirata KI, Rikitake Y. Involvement of aquaporin-4 in laminin-enhanced process formation of mouse astrocytes in 2D culture: roles of dystroglycan and alpha-syntrophin in aquaporin-4 expression. *J Neurochem*. 2018;147:495–513.
60. Sun H, Liang R, Yang B, et al. Aquaporin-4 mediates communication between astrocyte and microglia: Implications of neuroinflammation in experimental Parkinson's disease. *Neuroscience*. 2016;317:65–75.
61. Nakanishi M, Niidome T, Matsuda S, Akaike A, Kihara T, Sugimoto H. Microglia-derived interleukin-6 and leukaemia inhibitory factor promote astrocytic differentiation of neural stem/progenitor cells. *Eur J Neurosci*. 2007;25:649–658.
62. Tomar A, Lawson C, Ghassemian M, Schlaepfer DD. Cortactin as a target for FAK in the regulation of focal adhesion dynamics. *PLoS One*. 2012;7:e44041.
63. Cao H, Chen J, Krueger EW, McNiven MA. SRC-mediated phosphorylation of dynamin and cortactin regulates the "constitutive" endocytosis of transferrin. *Mol Cell Biol*. 2010;30:781–792.
64. Fan L, Di Ciano-Oliveira C, Weed SA, et al. Actin depolymerization-induced tyrosine phosphorylation of cortactin: the role of Fer kinase. *Biochem J*. 2004;380:581–591.
65. Head JA, Jiang D, Li M, et al. Cortactin tyrosine phosphorylation requires Rac1 activity and association with the cortical actin cytoskeleton. *Mol Biol Cell*. 2003;14:3216–3229.

Investigative Ophthalmology & Visual Science

66. Cho S, Muthukumar AK, Stork T, Coutinho-Budd JC, Freeman MR. Focal adhesion molecules regulate astrocyte morphology and glutamate transporters to suppress seizure-like behavior. *Proc Natl Acad Sci U S A*. 2018;115:11316–11321.

67. Morrison JC. Integrins in the optic nerve head: potential roles in glaucomatous optic neuropathy (an American Ophthalmological Society thesis). *Trans Am Ophthalmol Soc*. 2006;104:453–477.

68. Mullins RD, Hansen SD. In vitro studies of actin filament and network dynamics. *Curr Opin Cell Biol*. 2013;25:6–13.

69. Oser M, Mader CC, Gil-Henn H, et al. Specific tyrosine phosphorylation sites on cortactin regulate Nck1-dependent actin polymerization in invadopodia. *J Cell Sci*. 2010;123:3662–3673.

70. Kuehn MH, Kim CY, Ostojic J, et al. Retinal synthesis and deposition of complement components induced by ocular hypertension. *Exp Eye Res*. 2006;83:620–628.

Investigative Ophthalmology & Visual Science